Progress in Chemical and Biochemical Research

Journal homepage: www.pcbiochemres.com

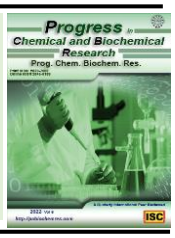

Original Research Article

Combined QSAR Modeling, Molecular Docking Screening, and Pharmacokinetics Analyses for the Design of Novel 2, 6-Diarylidene Cyclohexanone Analogs as Potent Anti-Leishmanial Agents

Fabian Audu Ugbe*, Gideon Adamu Shallangwa, Adamu Uzairu, Ibrahim Abdulkadir

Department of Chemistry, Faculty of Physical Sciences, Ahmadu Bello University, P.M.B. 1044, Zaria, Kaduna State, Nigeria

ARTICLE INFO

Article history

Submitted: 2022-10-20
Revised: 2022-12-03
Accepted: 2022-12-24
Available online: 2023-01-21
Manuscript ID: PCBR-2210-1234
DOI: 10.22034/pcbr.2022.366493.1234

KEYWORDS

Leishmaniasis
Diarylidene cyclohexanone
2-DQSAR
Molecular docking
Pharmacokinetics
Molecular dynamics

ABSTRACT

The current research was conducted as part of the anti-leishmanial drug discovery effort towards new drug molecules with attributes that overcome the limitations of existing therapies. This work utilizes a combined approach of Quantitative Structure-Activity Relationship (QSAR), virtual docking screening, and pharmacokinetics analysis to design some novel 2,6-diarylidene cyclohexanone analogs using ligand-based drug design methods, while also performing docking investigation, drug-likeness analysis, and Molecular Dynamic (MD) simulation to evaluate their anti-leishmanial potential. Some crucial parameters were calculated for the built QSAR model, including R^2 = 0.7827, R^2_{adj} = 0.7206, Q^2cv = 0.6414, and R^2_{test} = 0.8539, which indicate an acceptable QSAR model. The combined results of QSAR, docking, and pharmacokinetics analysis suggested compound **1** as the template. The Six (6) newly designed analogs possessed higher binding scores than the reference drug Pentamidine in the order; **1a** (-10.2 kcal/mol) > **1e** (-9.6) > **1d** (-9.4) > **1c** (-9.2) > **Template** (-9.1) > **1f** (-9) > **1b** (-8.5) > Pentamidine (-6.9 kcal/mol), while their predicted pIC_{50} followed the order; **1e** (8.7321) > **1c** (7.6772) > **1f** (7.1602) > **1a** (6.8289) > **1d** (6.7738) > **1b** (6.5772) > **Template** (5.3824). The results of the drug-likeness testing suggest **1** and the new analogs (especially **1a**) as being orally bioavailable with excellent pharmacokinetic profiles. These molecules equally showed good pharmacological interactions with the receptor, Pyridoxal kinase (PDB: 6K91). In addition, the MD simulation results confirmed the stability and rigidity of **1_6K91** and **1a_6K91**. Therefore, the new analogs could be considered as potent anti-leishmanial inhibitors.

* Corresponding author: Fabian Audu Ugbe
✉ E-mail: ugbefabianaudu@gmail.com
© 2022 by SPC (Sami Publishing Company)

GRAPHICAL ABSTRACT

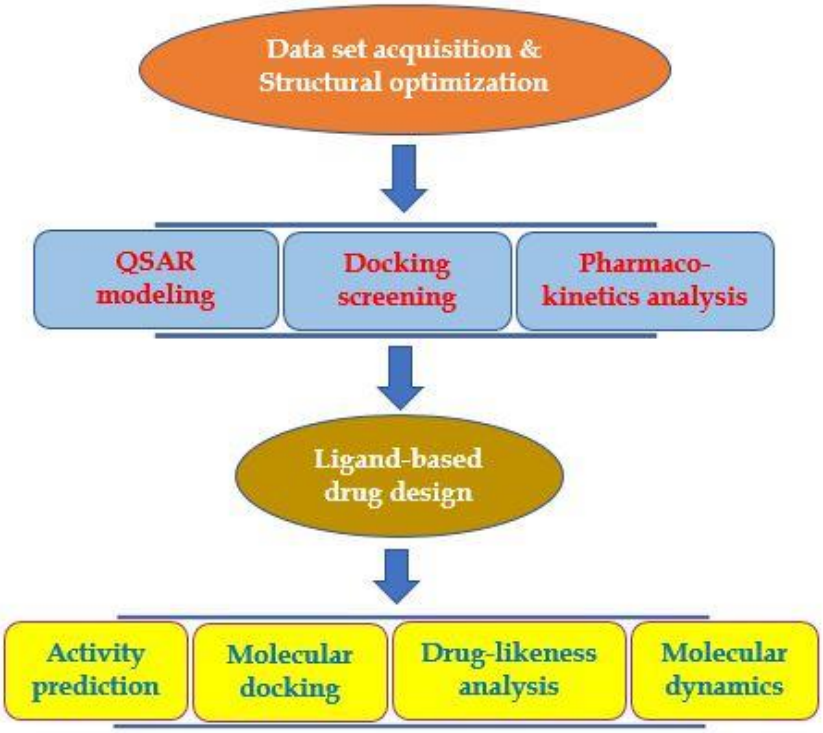

Introduction

Leishmaniasis, a neglected tropical disease is known to infect over 12 million people mainly in tropical Africa, Southeast Asia, and Latin America [1]. Visceral leishmaniasis (VL) is the deadliest of all leishmanial infections and always proves fatal if left untreated. VL is caused by the leishmanial (L) parasites majorly L. donovani and L. infantum transmitted by the female sand flies [2]. Major health conditions associated with leishmaniasis include weight loss, weakness, fever, and hepatosplenomegaly [3]. Due to the lack of a vaccine to prevent this infection, a major treatment approach has been the use of chemotherapy with drugs such as amphotericin B, pentamidine, paromomycin, and miltefosine among others [4]. However, these therapies are either not effective enough or are associated with adverse effects such as nausea, hepatotoxicity, nephrotoxicity, eye irritation, lethargy, and cardiotoxicity [5,6]. More so, resistance posed by target organisms to existing therapies is on the rise [7]. In addition, leishmaniasis is taken less seriously than other infections such as cancer, diabetes, malaria, stroke, hepatitis, and AIDS [8]. Therefore, it has become a necessity to discover and develop new medicines that overcome the limitations of existing therapies.

Computer-aided modeling approaches such as Quantitative Structure-Activity Relationship (QSAR), molecular docking investigation, pharmacokinetics properties prediction, and molecular dynamics simulation, amongst others play a crucial role in drug discovery and development owing to their merits over traditional methods such as time-saving, cost-effectiveness, and reliability [9,10]. The QSAR methodology is based on the concept that the differences observed in the biological activities of a series of compounds can be quantitatively correlated with differences in their molecular structures [11]. Molecular docking as an *in silico* screening method tends to probe the binding of ligands in the active sites of protein targets using

a valid docking tool [12]. Pharmacokinetics analysis as part of a drug optimization process is necessary during the pre-clinical phase of drug development to evaluate how new drug compounds will affect the living organism when administered. Some pharmacokinetic properties usually predicted during the theoretical study include Topological Polar Surface Area (TPSA), lipophilicity indices, and Absorption, Distribution, Metabolism, Excretion, and Toxicity (ADMET) [12, 13]. Likewise, physicochemical properties such as molecular weight, TPSA, lipophilicity, Hydrogen Bond Donors (HBD), and Hydrogen Bond Acceptors (HBA) are necessary to predict the oral bioavailability of a drug [14]. Lastly, Molecular Dynamic (MD) simulation is necessary to probe the stability and rigidity of protein-ligand interactions during a trajectory [15].

The pyridoxal kinase (PdxK) protein (PDB: 6K91) was reported previously to play a key role in the formation of pyridoxal -5'-phosphate, an active form of vitamin B6 by catalyzing the phosphorylation of the 5'-hydroxyl group of the pyridoxal [16]. PdxK is a key enzyme for the growth of parasites and is also useful in host infection [17]. Some well-known anti-malarial medicines such as primaquine and chloroquine have previously been reported to show inhibition against PdxK [17]. Hence, PdxK, the chosen biological target for this study, could serve as an interesting enzyme target for new leishmanial inhibitors.

Bis-(arylmethylidine)-cycloalkanones have been reported to show a wide range of activities such as anti-tumor, anti-tubercular, anti-inflammatory, and anti-oxidants [18]. The two aromatic moieties in bis-aryl-α, β unsaturated ketones have also been reported as important for the potential binding of the ligands to a given target protein [19]. However, the literature account of the computational exploration of the diarylidene cyclohexanone series as anti-leishmanial agents is missing. As part of an effort to discover a more effective anti-leishmanial agent to overcome the toxicological limitations of existing therapies and resistance posed by target organisms, a series of 2,6-diarylidene cyclohexanone were explored computationally to ascertain their effectiveness and suitability for use as superior leishmanial inhibitors. This study was focused on a combined virtual molecular docking screening and 2-Dimensional (2D) QSAR modeling to design some substituted 2,6-diarylidene cyclohexanone analogs, while also performing pharmacokinetic analysis and molecular dynamic simulation to establish their drug-likeness status and stability of the resulting ligand-protein complexes, respectively.

Materials and Methods

Data collection

Din *et al.* [18] synthesized a series of symmetrical and unsymmetrical substituted 2,6-diarylidene cyclohexanone analogs, as part of the anti-leishmanial drug discovery effort. Their inhibitory activities were measured against promastigotes of *L. amazonensis* and reported in micromolar (μM). Consequently, a dataset of Twenty-eight (28) compounds with relatively better half-maximal inhibitory concentration (IC_{50}) values were obtained from their report and used for this study. The molecular structures, bioactivities (IC_{50}), and pIC_{50} obtained as a logarithmic function of IC_{50} for these compounds were reported in the supplementary file, as listed in Table S1.

Hardware and software

An HP laptop computer with the following specifications was used: Processor (Intel(R) Core(TM) i5-4210U CPU @ 1.70GHz 2.40 GHz), Installed RAM (8.00 GB), System type (64-bit operating system, x64-based processor), Edition (Windows 10 Home Single Language), Version 21H2. The software includes Chemdraw Ultra v. 12.0.2, Spartan '14 v. 1.1.4, PaDEL-descriptor v. 2.20, and Drug Theoretics and Cheminformatics

Laboratory (DTC Lab) based software. Others include Material Studio v. 8.0, PyRx – Virtual Screening Tool, Biovia Discovery Studio Visualizer v. 16.1.0.15350, NAMD v 2.14, and VMD v 1.9.3 OpenGL Display [8-10].

Geometry optimization

The ChemDraw Ultra software was used to draw the molecular structures of the various analogs and thereafter saved in MDL molfile. The resulting files were opened separately on the Spartan '14 user interface and converted from 2-D to 3-D models. The resulting structures were subjected to a two-step optimization process; first with Molecular Mechanics Force Field (MMFF) and thereafter with Density Functional Theory (DFT) using B3LYP/6-31G** basis set. The resulting structures were then preserved in an SD file for use in the generation of molecular descriptors [10,20].

2D QSAR model building

The PaDEL-Descriptor tool helped generate a pool of molecular descriptors for all twenty-eight (28) compounds [10]. DTC-Lab-based pretreatment software, GUI 1.2 was used to treat and screen the data of uninformative descriptors [9]. The pretreated data were divided into a training set and a test set in a 70:30 proportion [21]. The actual model building was carried out on the Material studio software which employs the Genetic Function Approximation (GFA) and Multi-Linear Regression (MLR) approach to build the QSAR model. MLR provides the relationship between the inhibitory activity (pIC_{50}) and the molecular descriptors [22].

The next important step after the model building is internal and external validation assessment. Some internal validation parameters utilized in this study include correlation coefficient (R^2), cross-validation coefficient (Q^2cv), and adjusted correlation coefficient (R^2_{adj}). An external validation assessment was carried out to ascertain the built model's ability to predict the activities of the external test set compounds. The predictive strength of the QSAR model is dependent on the external test set correlation coefficient (R^2_{test}) [23-26]. In addition, statistical parameters such as the Mean Effect (ME) and Variance Inflation Factor (VIF) were computed to further describe the built QSAR model. The ME value shows the contribution of each descriptor in the model in terms of anti-proliferative activity [27], while the inter-correlation level between the descriptors is defined by the VIF [28]. Furthermore, the Applicability Domain (AD) space of the model was described using the leverage approach [29,30]. Table 1 indicates the various parameters and equations utilized in the model's validation.

Molecular docking screening

Molecular docking investigation was carried out separately between the target receptor (PdxK) and twenty-eight (28) compounds using the PyRx software (Auto Dock Vina tool). The screening was conducted to identify the ligands that bind very strongly with the target receptor. The receptor (PdxK) in 3-D form was obtained from the protein data bank and prepared on the Biovia Discovery Studio by removing water molecules and co-crystallized ligands associated with the protein structure. The 3D structures of all the ligands after their optimization were converted from Spartan to PDB files for use in molecular docking simulation [23, 27]. Figure 1 displays the 3D representation of compound **1** in the receptor's active sites.

Table 1. Selected equations and parameters used for the QSAR model validation

Parameter	Equation	Eq.	Threshold value	Reference
	Internal validation			
Friedman Lack-Of-Fit (LOF)	$LOF = \frac{SEE}{(1-\frac{c+d\,x\,p}{M})^2}$ $SEE = \sqrt{\frac{(Y_{exp}-Y_{pred})^2}{N-P-1}}$	1 2	-	[6]
Correlation Coefficient (R^2)	$R^2 = 1 - \left[\frac{\sum(Y_{exp}-Y_{pred})^2}{\sum(Y_{exp}-\bar{Y}_{training})^2}\right]$	3	≥ 0.6	[9]
Adjusted R^2	$R^2_{adj} = \frac{R^2 - p(n-1)}{n-p+1}$	4	≥ 0.5	[10]
Cross-validation regression coefficient (Q^2cv)	$Q^2_{cv} = 1 - \left[\frac{\sum(Y_{pred}-Y_{exp})^2}{\sum(Y_{exp}-\bar{Y}_{training})^2}\right]$	5	≥ 0.5	[10]
	External validation			
Predicted R^2 (R^2 test)	$R^2_{test} = 1 - \frac{\sum(Ypred_{test}-Yexp_{test})^2}{\sum(Ypred_{test}-\bar{Y}_{training})^2}$	6	≥ 0.6	[6]
	Pearson correlation and statistical analyses			
Mean Effect (ME)	$ME = \frac{B_j \sum_i^n D_j}{\sum_j^m (B_j \sum_i^n D_j)}$	7	-	[29]
Variance Inflation Factor (VIF)	$VIF = \frac{1}{(1-R^2)}$	8	≤ 10	[30]
Leverage (h) and warning leverage (h*)	$h = X(X^T X)^{-1} X^T$ $h^* = 3\frac{(j+1)}{m}$	9 10	- -	[31]

SEE = Standard Error of Estimation
c = no. of terms in the model
d = user-defined smoothing parameter
p = total no. of descriptors in the model
M = no. of data in the training set
$\bar{Y}$training = mean experimental activity of the training set
Yexp = experimental activity in the training set
Ypred = predicted activity in the training set
n = no. of compounds in the training set.
$Ypred_{test}$ = predicted activity of test set
$Yexp_{test}$ = experimental activity of test set
βj = coefficient of j descriptor
Dj = Descriptor's value for each molecule in the training set
m = j = no. of descriptors in the model
X = m x k descriptor matrix of the training set
X^T = transpose matrix of X

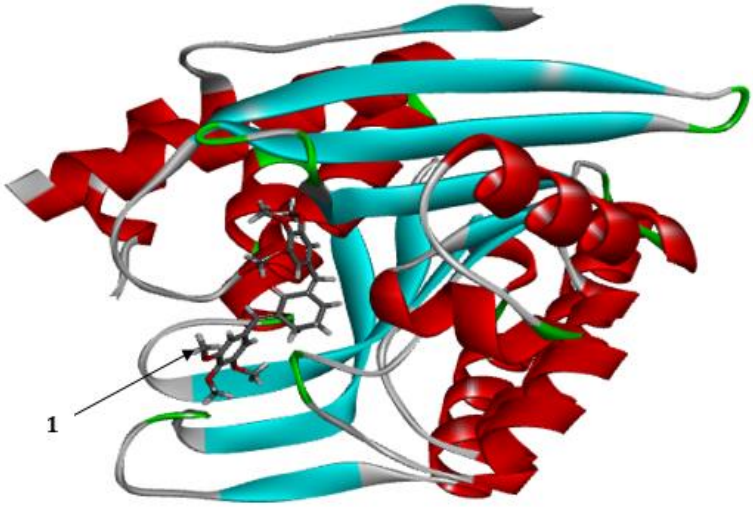

Figure 1. 3D representation of compound **1** in the active site of PdxK

Pharmacokinetics study

Pharmacokinetics profiling is important for an early drug discovery phase because only molecules that exhibit excellent drug-likeness properties advance into the pre-clinical phase of drug testing [10]. In the present study, the drug-likeness properties of some selected analogs (**1**, **2**, **3**, **7**, **22**, **26**, and **27**) were predicted using the online server, http://www.swissadme.ch/index.php. This was to determine which of the selected compounds would best be used as the design template. Lipinski's 'rule of five' (ROF), a widely applied criterion for oral bioavailability was used to assess the selected compounds for possible oral administration [14,31].

Ligand-based drug design

Six (6) new analogs of 2,6-diarylidene cyclohexanone were designed by the method of ligand-based drug design basically by careful inclusion of relevant substituent groups into the template structure (**1**) based on the information provided by the molecular descriptors (especially AATS6s and GATS3m) [9]. The newly designed compounds and reference drug (pentamidine) were prepared by the earlier described procedures. Like the selected analogs, the designed compounds were subjected to molecular docking investigation, and pharmacokinetics properties prediction to ascertain their mode of binding interactions and drug-likeness properties, respectively. To revalidate the docking results, pentamidine was equally docked onto the same binding pockets of PdxK (PDB: 6K91).

Molecular dynamics simulation and MM/GBSA calculation

The MD simulations were performed on the complexes of compound **1** (template) and compound **1a** with PdxK using the combined approach of Chemistry at Harvard Macromolecular Mechanics (CHARMM) force field, Nano-scale Molecular Dynamics (NAMD), and Visual Molecular Dynamics (VMD). The CHARMM-GUI, an established web-based platform that utilizes the CHARMM force field, was used to generate the input files for the simulation by NAMD [32]. The periodic boundary condition was utilized while fitting the system into a cubic water box for solvation. The protein was solvated and neutralized explicitly in an aqueous solution of 0.15M concentration of potassium chloride salt [33]. The simulation process involving energy minimization, equilibration (100 ps time frame), and production (2,500,000 steps or 5 ns time frame)

was performed on the resulting system, while the results were visualized using VMD and the Biovia discovery studio [34]. A similar procedure was described elsewhere [8, 33]. In addition, MolAICal software was used to compute the ligand-binding affinity by Molecular Mechanics Generalized Born Surface Area (MM/GBSA) method based on the resulting MD log files obtained with NAMD [35]. MM/GBSA is estimated using Equations (11) – (13) [28].

$$\Delta G_{bind} = \Delta H - T\Delta S \approx \Delta E_{MM} + \Delta G_{sol} - T\Delta S \quad (11)$$

$$\Delta E_{MM} = \Delta E_{internal} + \Delta E_{ele} + \Delta E_{vdw} \quad (12)$$

$$\Delta G_{sol} = \Delta G_{SA} + \Delta G_{GB} \quad (13)$$

Where, ΔE_{MM} is the gas phase MM energy, $-T\Delta S$ represents the conformational entropy, ΔE_{MM} is the sum of ΔE_{ele}, Van der Waals energy ΔE_{vdw} and $\Delta E_{internal}$ of bond, angle, and dihedral energies; ΔG_{sol} is the solvation free energy equal to the sum of the non-electrostatic solvation component ΔG_{SA}, and electrostatic solvation energy ΔG_{GB}.

Results and Discussion

QSAR modeling

A series of twenty-eight (28) 2, 6-diarylidene cyclohexanone derivatives were subjected to a 2D QSAR modeling to establish a quantitative relationship between their structures and their inhibitory activities. The built model (Equation 14) was assessed for both internal and external validation tests and was found to satisfy the criteria outlined for a good QSAR model. The four (4) molecular descriptors utilized in the QSAR model were described in Table 2, while the observed activities, predicted activities, and residual values were presented in Table 3. In addition, internal and external validation assessments were conducted to ascertain the robustness, reliability, and predictive strength of the QSAR model, with the results shown in Table 4.

A combined GFA and MLR approach led to the selection of 4 descriptors, and the generation of four (4) QSAR models, respectively. Model 4 (Equation 14) was found to best satisfy the requirement for a reliable QSAR model. The low residuals between the observed and predicted activities as shown in Table 3 indicate a high predictive strength of the model.

$$\boldsymbol{pIC_{50}} = 2.043304999 * \mathbf{AATS6s} + 0.106999746 * \mathbf{AATSC4v} - 4.341951406 * \mathbf{GATS3m} + 0.097618992 * \mathbf{RDF135m} + 3.781657162 \quad (14).$$

Table 2. Selected descriptors used in the QSAR model

S/No.	Descriptor	Description	Class	ME
1	AATS6s	Average Broto-Moreau autocorrelation - lag 6/weighted by I-state	2D	4.2856
2	AATSC4v	Averaged and centered Moreau-broto autocorrelation of lag 4 weighted by vdw volume	2D	-0.3830
3	GATS3m	Geary coefficient of lag 3 weighted by mass	2D	-3.0060
4	RDF135m	Radial Distribution Function - 13.5 / weighted by mass	2D	0.1033

Table 3. The observed pIC_{50}, predicted pIC_{50}, and residuals of 2,6-diarylidene cyclohexanone derivatives

Compound ID	AATS6s	AATSC4v	GATS3m	RDF135m	pIC_{50}	Pred.	Residual
1	2.83862	0.36492	0.97626	0.00421	5.5528	5.3824	0.1704
2	2.83544	-2.4836	0.95084	2.70589	5.4437	5.4452	-0.0015
3	2.81761	-3.2384	0.89377	2.75771	5.3768	5.5809	-0.2041
4*	3.25794	-0.8843	0.99707	0.12623	5.3665	6.0271	-0.6606
5*	2.88947	-4.7589	0.94868	1.00269	4.6576	5.1553	-0.4977
6	2.74786	-6.0592	0.82857	0.06698	5.3872	5.157	0.2303
7*	2.89511	-3.4525	0.83397	5.2E-06	5.3372	5.7068	-0.3695
8*	2.9516	-2.6897	0.84129	2.4E-08	5.3098	5.8720	-0.5622
9*	2.74695	3.74575	0.89377	2.46776	5.6383	6.1555	-0.5172
10	2.64295	-6.774	0.84499	1.79355	4.7696	4.9634	-0.1938
11*	2.6015	-7.2266	1.00587	5E-114	4.2676	3.9566	0.3110
12	2.75591	-3.966	0.9864	0.03635	4.9281	4.7091	0.2190
13	2.54971	-4.8292	1.04593	1.66688	4.0410	4.0961	-0.0552
14	2.78115	-5.6772	0.89287	0.15414	4.8861	4.9952	-0.1091
15	2.74652	-5.8343	0.9158	0.37761	4.7620	4.8299	-0.0679
16*	2.80639	-4.8954	0.8638	0.31222	5.2840	5.2721	0.0119
17	2.94326	-4.6395	0.99396	0.53154	4.9666	5.0354	-0.0688
18	2.71495	-2.6915	0.9158	0.30912	5.2441	5.095	0.1492
19	2.77963	-3.8465	0.88779	0.00487	4.7773	5.1955	-0.4182
20	2.77227	-6.0009	0.92226	1.05214	4.6968	4.9024	-0.2056
21	2.92639	-4.6286	0.90333	0.13125	5.3279	5.3565	-0.0286
22*	2.97678	-4.6237	0.8369	1.43084	5.4089	5.8753	-0.4663
23*	2.74754	-3.1438	0.92226	1.07063	4.7033	5.1594	-0.4561
24	2.69195	-6.4595	0.83691	6.36305	5.5850	5.5783	0.0067
25	2.88647	-7.5434	0.88395	0.29134	5.3188	5.0628	0.2559
26	2.51364	-2.9433	0.91832	3.5812	5.0000	4.9651	0.0349
27	2.65109	-6.9569	0.86922	4.6235	5.3468	5.1315	0.2153
28	2.81917	-5.2888	0.83271	8.28E-06	5.4318	5.3606	0.0712

Key: *test set compounds

A good QSAR model should have an R^2 value at least 0.60, R^2_{adj} not less than 0.50, Q^2_{cv} at least 0.50, a difference of R^2 and Q^2_{cv} not greater than 0.30, and R^2 for external test set not less than 0.60 [9, 10]. As reported in Table 4, the various parameters were predicted to satisfy the criteria specified by their thresholds for a good QSAR model. In addition, the built model showed a significant regression with the number of test set compounds being greater than 5. Pearson's correlation and other statistical analyses were performed on the selected descriptors and reported in Table 5. The values of correlation coefficients below 0.50 between any pair of descriptors show that no relationship exists between each pair of descriptors.

Table 4. Validated parameters of the QSAR model

Validation Parameters	Model	Threshold	Remarks
	Training set		
Friedman LOF	0.193957	-	-
R-squared (R^2)	0.782670	≥ 0.6	Passed
Adjusted R-squared (R^2_{adj})	0.720576	≥ 0.5	Passed
Cross-validated R-squared (Q^2_{cv})	0.641403	≥ 0.5	Passed
R^2 - Q^2_{cv}	0.141267	≤ 0.3	Passed
Significant Regression	YES	-	-
Significance-of-regression F-value	12.604567	-	-
Critical SOR F-value (95%)	3.160163	-	-
Replicate points	0	-	-
Computed experimental error	0.0000000	-	-
Number of Train set compounds	19	-	-
Min expt. error for non-significant LOF (95%)	0.15787500	-	-
		Test set	
R-squared (R^2_{test}) i.e. r^2	0.85393	≥ 0.6	Passed
Number of test set compounds ($N_{test\ set}$)	9	≥ 5	Passed

The VIF establishes the orthogonality of the descriptors in the model, with a value greater than 10 indicating that the descriptors' information may be hidden by the correlation of the other descriptors. Here, the VIF values for the various descriptors range between 1 and 5, which shows that the descriptors are fairly independent of each other (Table 5). The absolute t-statistics values of greater than 2 showed that the selected descriptors were good [36]. The evaluated p-values at a 95% confidence level for various descriptors were < 0.05, indicating that a relationship exists between binding activities and the descriptors. Furthermore, the Mean Effect (ME) values reported in Table 2 indicate the contributory strength of each descriptor in the model. The strength and direction of contributions by the respective descriptors on the molecules' inhibitory activities are signified by the magnitudes and signs of their ME values. AATS6s and RDF135m have positive ME values, meaning that an increase or a decrease in their values will result in an increase or decrease in the inhibitory activities, respectively. Increasing values of AATSC4v and GATS3m, on the other hand, will lead to a decrease in the anti-leishmanial activities because both descriptors have negative ME values. AATS6s has the largest influence on the molecules' inhibitory activities because it has the highest ME value of 4.2856. AATS6s which is the Average Broto-Moreau autocorrelation - lag 6 weighted by I-state, was suggested to contribute positively to anti-leishmanial activity [6].

Table 5. Pearson's correlation and statistical analyses of descriptors used in the QSAR model

Descriptors	Inter-correlation				Statistical parameters		
	AATS6s	AATSC4v	GATS3m	RDF135m	VIF	t Stat	p-value
AATS6s	1				1.3380	4.1591	0.0010
AATSC4v	0.10008	1			1.3498	3.6884	0.0024
GATS3m	-0.0012	0.49847	1		1.3902	-4.5060	0.0005
RDF135m	-0.4853	-0.17364	-0.21129	1	1.3906	3.1325	0.0073

The plot of standardized residuals against the leverages also called William's plot was obtained to determine the model's applicability domain (Figure 2). As observed from the plot, all the molecules fall within the square area ±2.5, which showed no presence of an outlier in the data set. However, two compounds (**4** and **9**) were found beyond the cut-off leverage (h* = 0.79) and were regarded as influential molecules.

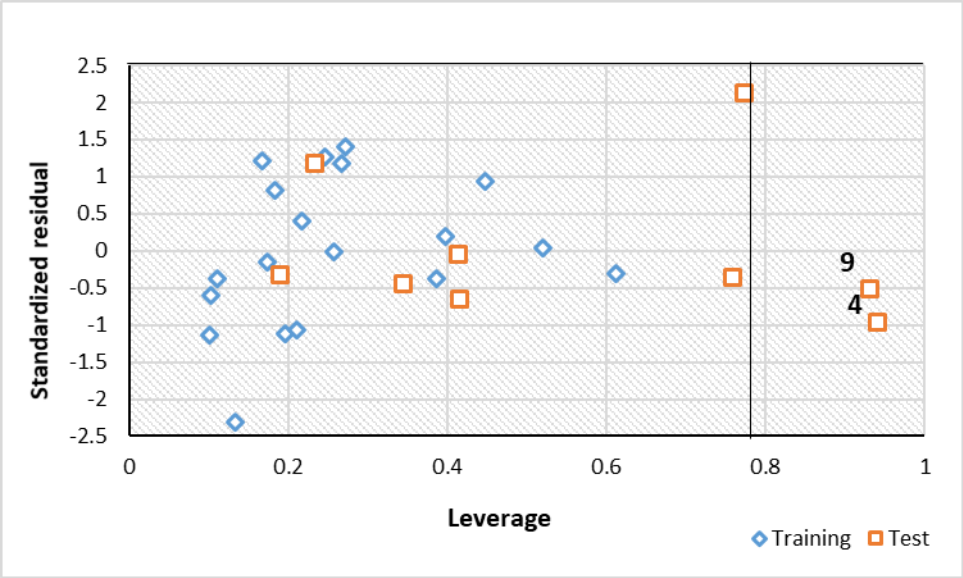

Figure 2. The plot of standardized residuals versus leverages (William's plot)

As a result, compounds **1**, **2**, **3**, **7**, **22**, **26**, and **27** with relatively higher predicted activities (Table 3), being also found within the built model's applicability domain (Figure 2), and with low residuals were selected for pharmacokinetics testing to ascertain their oral bioavailability and drug-likeness properties.

Virtual docking screening

The results (binding affinities) of the docking simulation conducted between PdxK and the various diarylidene cyclohexanone analogs were reported in the supplementary file Table S1. The binding score which is a measure of the degree of affinity between a ligand and a receptor is most often used in the screening of a large library of compounds to find more active molecules that interact strongly with a receptor of interest. Binding affinities of the protein-ligand interactions are necessary to describe how strongly the drug compound binds to the target macromolecule. The negative value of the binding energy change shows the spontaneity and favorability of the binding process and how well ligands can fit into the target protein pocket to form the most energetically stable drug receptor [10]. The binding affinities available in

Table S1 range from -7.5 kcal/mol to -11 kcal/mol, with compounds **5** and **10** showing the highest and lowest negative binding scores of -11 kcal/mol and -7.5 kcal/mol, respectively. All the compounds selected for further evaluation from the QSAR study (**1**, **2**, **3**, **7**, **22**, **26**, and **27**) showed negative binding scores of greater than -9 kcal/mol, which were higher than the average binding score of -8.8 kcal/mol and the binding score of -6.9 kcal/mol reported for the reference compound, pentamidine. A similar observation was reported elsewhere for molecular docking investigation of some analogs of the arylimidamide-azole hybrid [4] and arylbenzimidazole [37] series. Compound **5** was not considered due to its relatively lower predicted inhibitory activity. In this study, the molecular docking screening was a follow-up on the QSAR study to further scrutinize the initially selected analogs, and consequently, all the selected analogs progressed into the next evaluation phase (drug-likeness testing).

Pharmacokinetics study

The results of the pharmacokinetics investigation conducted on the seven (7) selected analogs were presented in the Supplementary file, as indicated in Table S2, while Figure S1 shows their boiled egg representation.

Lipinski's approach to ascertaining the oral bioavailability of compounds has been widely applied in the discovery of new drug molecules [10]. It is mentioned that a drug molecule is likely to be orally bioavailable when HBD is less than 5, HBA < 10, MW < 500, and MLOGP < 4.15 or WLOGP < 5 [14]. A molecule that passed at least three of four provisions of the rule is said to be orally bioavailable [38]. As observed in Table S2, all the tested analogs passed the drug-likeness test (ROF) with only one violation (that is, MLOGP > 4.15). The reported values of TPSA for the molecules were less than 140 $Å^2$ (the threshold value for TPSA), above which molecules tend to exhibit poor Gastro-Intestinal (GI) absorption. Likewise, the synthetic accessibility scores of various compounds were less than 5.00 (easy portion on a scale of 1 to 10), suggesting their easy laboratory synthesis. The estimated water solubility (Log S) of the various molecules suggests poor solubility for various analogs except compound **1** predicted to be moderately soluble in aqueous media.

The estimated GI absorption was high for all tested compounds except compound **3**. Furthermore, only compounds **1**, **26**, and **27** were predicted to permeate through the Blood-Brain Barrier (BBB), while none of the tested molecules were predicted to be Central Nervous System (CNS) permeable. The boiled egg representation (Figure S1) confirmed that only **1**, **26**, and **27** are BBB permeants. Furthermore, all the tested molecules are non-substrates of P-glycoprotein, an enzyme acting as a biological barrier by extruding toxins and xenobiotics, including drugs out of cells. This means that these molecules when taken into the body may not be effluated from the target cells by this enzyme. This was confirmed by the red dots representation of these analogs in Figure S1. In addition, some special enzymes called cytochrome P450 enzymes are important in the body to aid the metabolism of drugs and to facilitate their excretion. Some tested isoforms include CYP-34A, CYP-2D6, CYP-1A2, CYP-2C19, and CYP-2C9. All the compounds were predicted as substrates of CYP-2C9, and non-substrates of CYP-1A2 and CYP-34A. Moreover, all tested analogs were predicted as substrates of CYP-2C19 except **1** and **3**, while only 1 is a substrate of CYP-2D6. Various molecules had therefore demonstrated abilities to aid their metabolism in the body. Based on the results of this study, compound **1** is considered to possess the best pharmacokinetics profile most especially because of its solubility. Hence, compound **1** was the preferred template molecule for the design of novel analogs.

Ligand-based drug design

One of the main objectives of the ligand-based drug design is to design new agents with better inhibitory activities than the design template. The molecular structures, predicted pIC_{50}, and binding affinities (kcal/mol) of the newly designed compounds as well as pentamidine were presented in Table 6. The predicted pIC_{50} values of the 6 newly designed analogs (**1a** – **1f**) were higher than that of the template molecule (**1**) in the order: **1e** (8.7321) > **1c** (7.6772) > **1f** (7.1602) > **1a** (6.8289) > **1d** (6.7738) > **1b** (6.5772). Therefore, it affirmed that the various structural modifications of the template structure yielded the desired result as it was based on the information encoded by the molecular descriptors in the built model. The binding affinities of the newly designed compounds range from -8.5 kcal/mol to -10.2 kcal/mol in the order: **1a** (-10.2 kcal/mol) > **1e** (-9.6 kcal/mol) > **1d** (-9.4 kcal/mol) > **1c** (-9.2 kcal/mol) > **Template** (-9.1 kcal/mol) > **1f** (-9 kcal/mol) > **1b** (-8.5 kcal/mol), and were higher than that of the reference compound, pentamidine (-6.90 kcal/mol).

Table 6. Molecular structures, predicted pIC_{50}, and binding affinities of newly designed analogs

Compound ID	Molecular structures	Predicted activity	Binding affinity
Template (1)	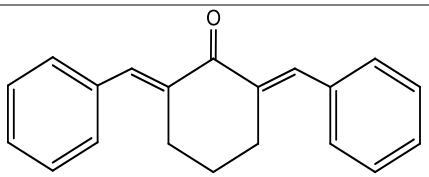	5.3824	-9.10
1a	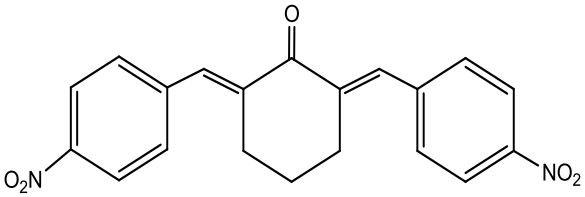	6.8289	-10.20
1b	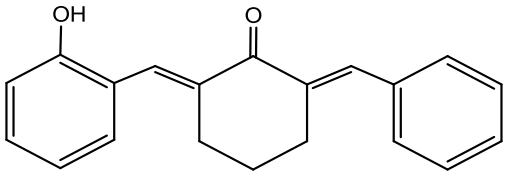	6.5772	-8.50
1c	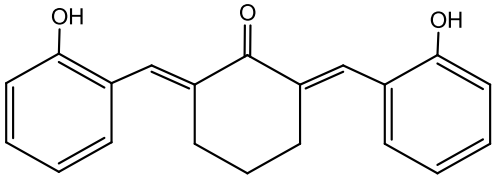	7.6772	-9.20
1d	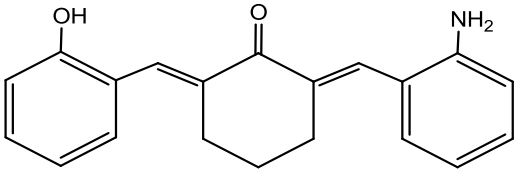	6.7738	-9.40

1e	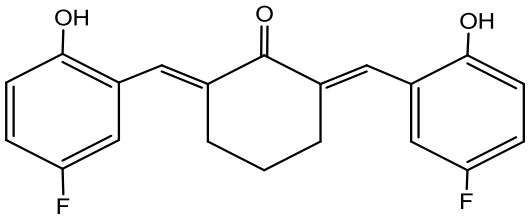	8.7321	-9.60
1f	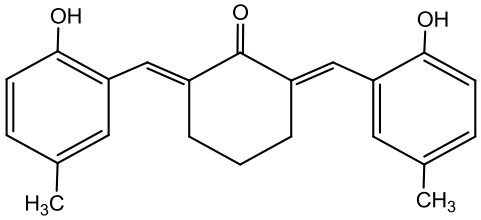	7.1602	-9.00
Pentamidine	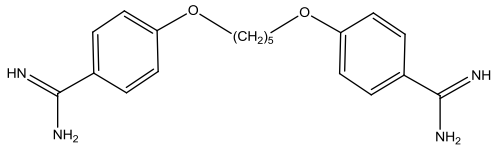	-	-6.90

The results of the pharmacokinetics investigation conducted on the six (6) newly designed analogs were presented in the Supplementary file, Table S3, while Figure S2 showed their boiled egg representation.

The results of the pharmacokinetic properties available in Table S3 showed a great improvement over those of the template molecule, being that the new analogs obeyed the ROF without any violation, and also are substrates to most of the cytochrome P450 enzymes that facilitate drug metabolism in the body. Like the lead molecule, the new analogs were predicted to be moderately soluble in aqueous media. In conclusion, the newly designed compounds have shown remarkable improvement over the designed template in the various areas investigated including binding activity, binding affinity, and pharmacokinetics properties.

Pharmacological interaction study

The binding interactions between the protein's amino acid residues and the newly designed compounds including the template (**1**) and the reference compound (pentamidine) were summarized in the supplementary file Table S4, while the binding interactions of **1**, **1a**, and pentamidine with PdxK were shown in Figures 3, 4, and 5, respectively. This was to provide insight into the binding interaction patterns of these ligands with the active sites of the target protein (PdxK). The choice of **1a** (pIC_{50} = 4.6983) was based on its excellent pharmacokinetic properties over the others, as well as improved inhibitory activity over the template, and its best binding affinity of -10.2 kcal/mol. Therefore, the discussion on pharmacological interactions shall be limited to the template compound (**1**) and **1a**.

The various compounds were mentioned to interact very strongly with the target receptor as shown by the presence of hydrogen bonding (H-bond), hydrophobic interactions, and in some cases electrostatic interactions (Table S4). The binding profile of compound **1** with PdxK involved a total of Three (3) conventional H-bonds and up to Three (3) hydrophobic interactions. Carbonyl group (C=O) oxygen of the cyclohexanone ring played a significant role in the formation of 3 conventional H-bonds with THR-229 at interaction distances of 2.52Å and 2.56Å, and GLY-230 at 1.93Å. The hydrophobic interactions include π-π T-shaped and π-sigma with HIS-46 and VAL-19, respectively, via one of the phenyl π-electron systems, and alkyl interaction with VAL-121 via C-4 carbon of the

cyclohexanone ring system. As seen in Figure 3, there's a tremendous improvement in the binding interaction profile of **1a** over that of **1**. Visible in the binding profile of **1a,** were seven (7) conventional H-bonds and two (2) hydrophobic interactions. The larger number of H-bond interactions in **1a**_PdxK was a result of the incorporation of the di-nitro group into the structural template, which accounted for the additional 4 H-bonds. The H-bonds were formed with HIS-46, GLY-48, and SER-47 at 2.26 Å, 2.78 Å, and 2.68 Å respectively, via one of the nitro group oxygen; THR-229 and GLY-230 at 2.85 Å, 3.62 Å, and 1.76 Å via the carbonyl group (C=O) oxygen of the cyclohexanone ring; and SER-188 at 1.92 Å via the other nitro group. Therefore, compound **1a** is mentioned to compete favorably well with the reference drug, pentamidine in terms of their interactions with the protein (6K91). The binding interaction profiles of the other newly designed compounds (**1b** – **1f**) were presented in the Supplementary file, as demonstrated in Figures S3-S7.

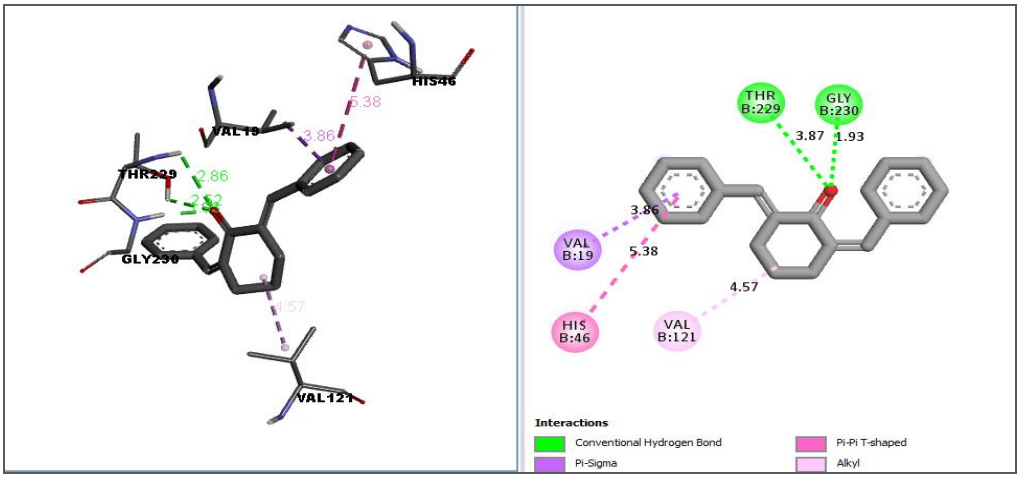

Figure 3. Binding interactions of compound **1** with PdxK.

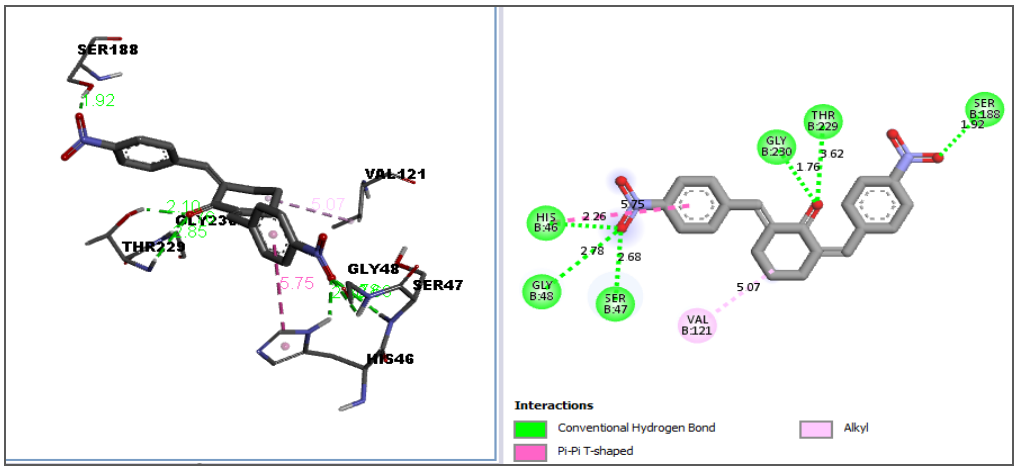

Figure 4. Binding interactions of compound **1a** with PdxK.

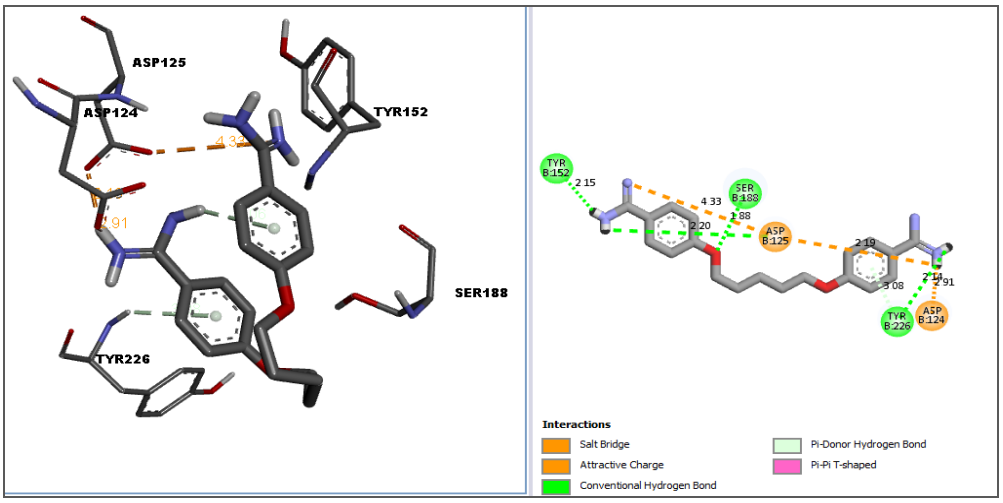

Figure 5. Binding interactions of Pentamidine with PdxK

Molecular dynamics study and calculation of MM/GBSA

A Molecular dynamics simulation study is necessary to ascertain the stability and rigidity of the protein-ligand interactions. As a result, the complexes of compounds **1** (template) and **1a** were subjected to the MD simulation, while the results summarized as plots of Root-Mean-Square Deviation (RMSD) and Radius of gyration (Rg) versus the time in picoseconds (ps) were presented in the supplementary file Figures S8 and S9 respectively.

The average RMSD values were estimated as 6.9874Å for **1**_6K91 and 5.1251Å for **1a**_6K91 which showed that **1a**_6K91 deviated less than **1**_6K91 (Figure S8), an indication of more stability for **1a**_6K91 [26]. The Rg measures the degree of protein's compactness during the trajectory. Decreasing Rg indicates reducing residues' flexibilities and more stability for the protein. Throughout the trajectory, the Rg varies between 18.10 Å and 18.80 Å which is equivalent to a difference of less than 0.8 Å for the complexes studied, connoting only a slight change in the protein compactness as the simulation progresses, which therefore indicates the stability of the complexes (Figure S9). Furthermore, the result of binding free energy (MM/GBSA) computed for **1**_6K91 and **1a**_6K91 by MolAICal is shown in Table 7.

Table 7. Binding free energy parameters of **1_6K91** and **1a_6K91** complexes

Energy (kcal/mol)	1_6k91	1a_6k91
ΔE (internal)	12.0423	1.2333
ΔE (electrostatic) + ΔG(solvation)	-28.5490	-29.0774
ΔE (Van der Waals)	-40.9152	-42.5481
ΔG binding (MM/GBSA)	-57.4219	-70.3922

The negative value of the estimated binding free energy (MM/GBSA) for both complexes (**-57.4219** kcal/mol and **-70.3922** kcal/mol for **1**_6K91 and **1a**_6K91, respectively) shows the favorability of the ligand-protein binding. The higher binding free energy associated with **1a**_6K91 is an indication that it is more energetically stable and binds more strongly with the receptor. A similar observation was reported elsewhere for binding free energy change (MM/GBSA) calculated for some analogs of 2-arylbenzimidazole in a complex with PdxK [37].

To further confirm the stability of the ligand-protein interactions during the simulation, the complexes were viewed using the Biovia discovery studio, and the resulting binding interactions were presented in Figures 6 and 7 for **1**_6K91 and **1a**_6K91, respectively. It became obvious that the conventional H-bond interactions were lost following the dynamic simulation of both complexes. However, the Carbon-hydrogen bond (GLY-48 at 2.92Å), π-anion electrostatic interaction (ASP-124 at 4.99Å), and hydrophobic interactions were visible in the binding profile of **1a**_6K91 (Figure 7). On the other hand, only hydrophobic interactions (VAL-19, VAL-121, and LYS-187) were visible in the binding profile of **1**_6K91 (Figure 6). It can therefore be inferred that compound **1a** binds more readily with PdxK, and hence could be considered potentially suitable for the treatment of leishmanial infections.

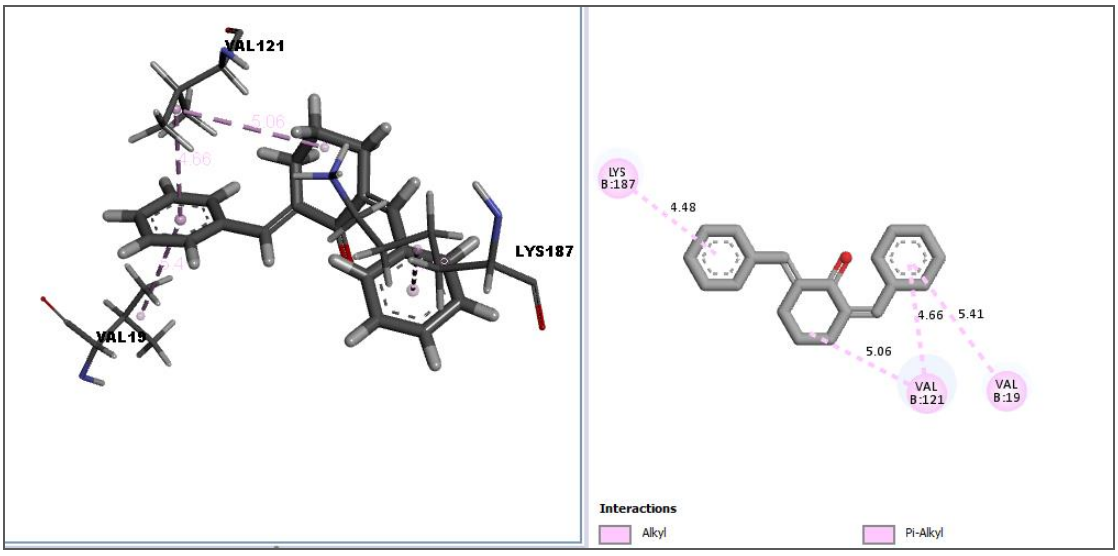

Figure 6. Binding interactions of compound **1** with PdxK after MD simulation

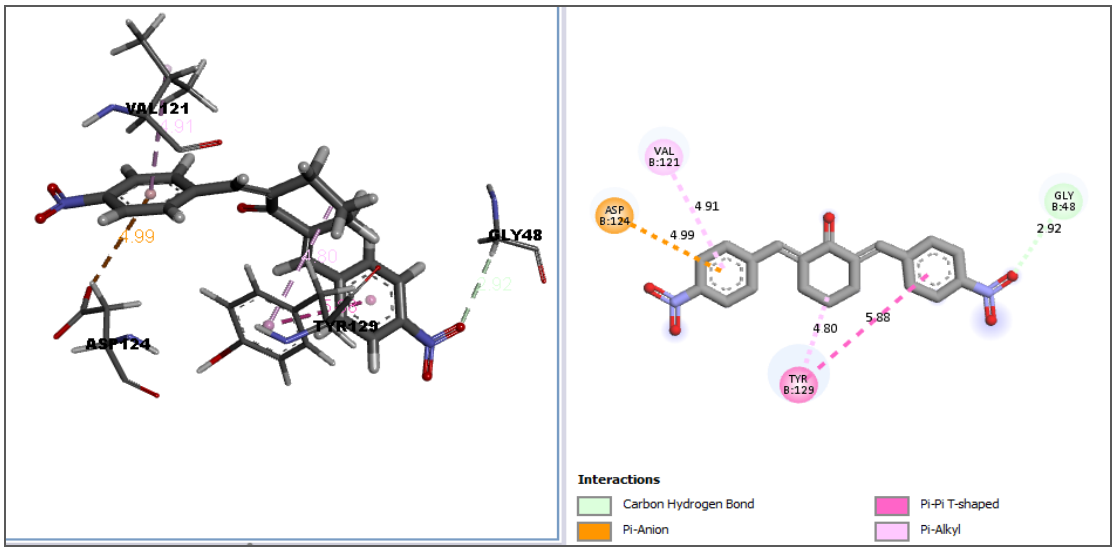

Figure 7. Binding interactions of compound **1a** with PdxK after MD simulation.

Conclusion

In this study, a four-descriptor QSAR model was built with twenty-eight (28) diarylidene cyclohexanone analogs and was found to satisfy the requirement for both internal and external validation tests with squared correlation coefficient (R^2) values of 0.7827 and 0.8540, respectively. The anti-leishmanial activities of the various compounds were well-predicted by the built QSAR model. The ligand-based drug design approach was used to design and predict the binding activities of six (6) new diarylidene cyclohexanone analogs (**1a**-**1f)**. The molecular docking screening performed between the 28 diarylidene cyclohexanone compounds and the target receptor, Pyridoxal Kinase (PdxK) revealed compounds **5** and **10** having the highest and lowest negative binding scores of -11 kcal/mol and -7.5 kcal/mol, respectively, both higher than the binding score of -6.9 kcal/mol reported for the reference drug pentamidine. Compound **1** was considered to possess the best pharmacokinetics profile and was selected as the template molecule. The newly designed compounds bind excellently into PdxK's cavities with binding affinities in the order; **1a** (-10.2 kcal/mol) > **1e** (-9.6 kcal/mol) > **1d** (-9.4 kcal/mol) > **1c** (-9.2 kcal/mol) > **Template** (-9.1 kcal/mol) > **1f** (-9 kcal/mol) > **1b** (-8.5 kcal/mol), while their predicted pIC_{50} follows the order; **1e** (8.7321) > **1c** (7.6772) > **1f** (7.1602) > **1a** (6.8289) > **1d** (6.7738) > **1b** (6.5772) > **Template** (5.3824). In addition, the newly designed molecules showed excellent pharmacokinetic profiles and were predicted to be orally bioavailable. The predicted pharmacological interaction profiles of these compounds generally showed a good fitting into the target site cavities, especially **1a**. Furthermore, the MD simulation revealed the stability and rigidity of the ligand-protein interactions of **1** and **1a**. Hence, the newly designed molecules, especially **1a** could be developed and further evaluated as potential drug candidates for the treatment of leishmanial infections.

Acknowledgments

The authors sincerely acknowledge G.F.S Harrison Quantum Chemistry Research Group, Ahmadu Bello University Zaria, for their guidance and support during this work.

References

[1] L.D.C. Clementino, G.F.S. Fernandes, I.M. Prokopczyk, W.C. Laurindo, D. Toyama, B.P. Motta, Design, synthesis and biological evaluation of N-oxide derivatives with potent in vivo antileishmanial activity. *PLoS ONE*, 16 (2021) e0259008. https://doi.org/10.1371/journal.pone.0259008.

[2] A. Upadhyay, P. Chandrakar, S. Gupta, N. Parmar, S.K. Singh, M. Rashid et al., Synthesis, biological evaluation, structure–activity relationship, and mechanism of action studies of quinoline–metronidazole derivatives against experimental visceral Leishmaniasis. *J. Med. Chem.,* 62 (2019) 5655–5671.

[3] M.D. Yousuf, D. Mukherjee, A. Pal, S. Dey, S. Mandal, C. Pal et al., Synthesis and biological evaluation of Ferrocenylquinoline as a potential antileishmanial agent. *Chem. Med. Chem.,* 10 (2015) 546-554.

[4] F.A. Ugbe, G.A. Shallangwa, A. Uzairu, I. Abdulkadir, A combined 2-D and 3-D QSAR modeling, molecular docking study, design, and pharmacokinetic profiling of some arylimidamide-azole hybrids as superior L. donovani inhibitors. *Bull. Natl. Res. Cent.*, 46 (2022) 189. https://doi.org/10.1186/s42269-022-00874-1.

[5] C.C.B. Brito, H.V.C. da Silva, D.J. Brondani, A.R. de Faria, R.M. Ximenes, I.M. da Silva et al., Synthesis and biological evaluation of thiazole derivatives as LbSOD inhibitors. *Journal of Enzyme Inhibition and Medicinal Chemistry,* 34 (2019) 333-342.

[6] F.A. Ugbe, G.A. Shallangwa, A. Uzairu, I. Abdulkadir, Theoretical modeling and design of some pyrazolopyrimidine derivatives as Wolbachia inhibitors, targeting lymphatic flariasis and onchocerciasis. *In Silico Pharmacol.,* 10 (2022) 8. https://doi.org/10.1007/s40203-022-00123-3.

[7] Y. Fan, Y. Lu, X. Chen, B. Tekwani, X. Li, Y. Shen, Anti-Leishmanial and cytotoxic activities of a series of maleimides: synthesis, biological evaluation and structure-activity relationship. *Molecules*, 23 (2018) 2878. https://doi.org/10.3390/molecules23112878.

[8] F.A. Ugbe, G.A. Shallangwa, A. Uzairu, I. Abdulkadir, Theoretical activity prediction, structure-based design, molecular docking and pharmacokinetic studies of some maleimides against Leishmania donovani for the treatment of leishmaniasis. *Bull. Natl. Res. Cent.*, 46 (2022) 92. https://doi.org/10.1186/s42269-022-00779-z.

[9] S.E. Adeniji, D.E. Arthur, M. Abdullahi, A. Abdullahi, F.A. Ugbe, Computer-aided modeling of triazole analogues, docking studies of the compounds on DNA gyrase enzyme and design of new hypothetical compounds with efficient activities. J. Biomol. Struct. Dyn., 2020 (2020). https://doi.org/10.1080/07391102.2020.1852963.

[10] F.A. Ugbe, G.A. Shallangwa, A. Uzairu, I. Abdulkadir, Activity modeling, molecular docking and pharmacokinetic studies of some boron-pleuromutilins as anti-wolbachia agents with potential for treatment of filarial diseases. *Chemical Data Collections,* 36 (2021) 100783. https://doi.org/10.1016/j.cdc.2021.100783.

[11] L. Abdel-Ilah, E. Veljovic, L. Gurbeta, A. Badnjevic, Applications of QSAR study in drug design. *International Journal of Engineering Research and Technology,* 6 (6) (2017).

[12] M.T. Ibrahim, A. Uzairu, G.A. Shallangwa, S. Uba, Lead identification of some anti-cancer agents with prominent activity against Non-small Cell Lung Cancer (NSCLC) and structure-based design. *Chemistry Africa*, 3 (2020) 1023–1044.

[13] H.A. Lawal, A. Uzairu, S. Uba, QSAR, molecular docking studies, ligand-based design and pharmacokinetic analysis on Maternal Embryonic Leucine Zipper Kinase (MELK) inhibitors as potential anti-triple-negative breast cancer (MDA-MB-231cell line) drug compounds. *Bulletin of the National Research Centre*, 45 (90) (2021). https://doi.org/10.1186/s42269-021-00541-x.

[14] C.A. Lipinski, F. Lombardo, B.W. Dominy, P.J. Feeney, Experimental and computational approaches to estimate solubility and permeability in drug discovery and development settings. *Advanced Drug Delivery Reviews,* 46 (2001) 3-26.

[15] E.I. Edache, A. Uzairu, P.A. Mamza, G.A. Shallangwa, Theoretical investigation of the cooperation of iminoguanidine with the enzymes-binding domain of Covid-19 and bacterial lysozyme inhibitors and their pharmacokinetic properties. *J. Mex. Chem. Soc.,* 66(4) (2022) 513-542.

[16] S. Are, S. Gatreddi, P. Jakkula, I.A. Qureshi, Structural attributes and substrate specificity of pyridoxal kinase from Leishmania donovani. *Int. J. Biol. Macromol.,* 152 (2020) 812-827.

[17] V. Kumar, M. Sharma, B.R. Rakesh, C.K. Malik, S. Neelagiri, K.B. Neerupudi et al., Pyridoxal kinase: a vitamin B6 salvage pathway enzyme from Leishmania donovani. *Int. J. Biol. Macromol.,* 119 (2018) 320-334.

[18] Z.U. Din, M.A. Trapp, L. Soman de Medeiros, D. Lazarin-Bidóia, F.P. Garcia, F. Peron et al., Symmetrical and unsymmetrical substituted

2,5-diarylidene cyclohexanones as anti-parasitic compounds. *European Journal of Medicinal Chemistry*, 155 (2018) 596–608.

[19] H. Chandru, A.C. Sharada, B.K. Bettadaiah, C.S.A. Kumar, K.S. Rangappa, J.K. Sunila, In vivo growth inhibitory and anti-angiogenic effects of synthetic novel dienone cyclopropoxy curcumin analogs on mouse Ehrlich ascites tumor. *Bioorg Med Chem*., 15 (2007) 7696–703.

[20] X. Wang, H. Dong, Q. Qin, QSAR models on aminopyrazole-substituted resorcylate compounds as Hsp90 inhibitors. *J. Comp. Sci. & Eng.,* 48 (2020) 1146-1156.

[21] R.W. Kennard, L.A. Stone, Computer aided design of experiments. *Technometrics,* 11 (1969) 137–148.

[22] D.E. Arthur, A. Uzairu, P. Mamza, S.E. Abechi, G.A. Shallangwa, Activity and toxicity modeling of some NCI selected compounds against leukemia P388ADR cell line using genetic algorithm-multiple linear regressions. *Journal of King Saud University – Science,* 32 (2020) 324-331.

[23] S.N. Adawara, G.A. Shallangwa, P. Mamza, A. Ibrahim, Molecular docking and QSAR theoretical model for prediction of phthalazinone derivatives as new class of potent dengue virus inhibitors. *Beni-Suef University Journal of Basic and Applied Sciences*, 9 (2020). https://doi.org/10.1186/s43088-020-00073-9.

[24] Y. Isyaku, A. Uzairu, S. Uba, M.T. Ibrahim, A.B. Umar, QSAR, molecular docking, and design of novel 4-(N, N-diarylmethyl amines) Furan-2(5H)-one derivatives as insecticides against Aphis craccivora. *Bull. Natl. Res. Cent*., 44 (2020) 44. https://doi.org/10.1186/s42269-020-00297-w.

[25] K. Roy, P. Chakraborty, I. Mitra, P.K. Ojha, S. Kar, R.N. Das, Some case studies on application of "rm2" metrics for judging quality of quantitative structure–activity relationship predictions: Emphasis on scaling of response data. *J. Comp. Chem.,* 34 (2013) 1071-1082.

[26] E.I. Edache, H. Samuel, Y.I. Sulyman, O. Arinze, O.I. Ayine, QSAR and molecular docking analysis of substituted tetraketone and benzyl-benzoate analogs as anti-tyrosine: A novel approach to anti-tyrosine kinase drug design and discovery.*Chemistry Research Journal*, 5 (2020) 79-100.

[27] S.E. Adeniji, S. Uba, A. Uzairu, Activity modeling of some potent inhibitors against mycobacterium tuberculosis using genetic function approximation approach. *Adıyaman University Journal of Science,* 9 (2019) 77-98.

[28] A. Abdullahi, G.A. Shallangwa, M.T. Ibrahim, A.U. Bello, D.E. Arthur, A. Uzairu et al., QSAR studies on some C14-urea tetrandrine compounds as potent anti-cancer agents against Leukemia cell line (K562). *JOTCSA,* 5 (2019) 1391-402.

[29] A. Tropsha, P. Gramatica, V.K. Gombar, The importance of being earnest: validation is the absolute essential for successful application and interpretation of QSPR models. *Mol. Inform.,* 22 (2003) 69-77.

[30] R. Veerasamy, H. Rajak, A. Jain, S. Sivadasan, C.P. Varghese, R.K. Agrawal, Validation of QSAR models-strategies and importance. *Int. J. Drug. Des. Discov.,* 3 (2011) 511–519.

[31] Y. Sun, A.W. Yang, A. Hung, G.B. Lenon, Screening for a potential therapeutic agent from the herbal formula in the 4th edition of the Chinese national guidelines for the initial-stage management of COVID-19 via molecular docking. Evid Based Complement Alternat Med, (2020) 3219840. https://doi.org/10.1155/2020/3219840.

[32] J. Lee, X. Cheng, J.M. Swails, M.S. Yeom, P.K. Eastman, J.A. Lemkul et al., CHARMM-GUI input generator for NAMD, GROMACS, AMBER, OpenMM, and CHARMM/OpenMM simulations using the CHARMM36 additive

force field. *J. Chem. Theory Comput.,* 12 (2016) 405-413.

[33] E.I. Edache, A. Uzairu, P.A. Mamza, G.A. Shallangwa, Computational modeling and analysis of the theoretical structure of thiazolino 2-pyridone amide inhibitors for Yersinia pseudo-tuberculosis and Chlamydia trachomatis Infectivity. *Bull. Sci. Res.,* 4 (2022) 14-39.

[34] F. Muniba, Molecular dynamics (MD) simulation using Gromacs. *Bioinformatics Review*, 5 (2019) 12.

[35] Q. Bai, S. Tan, T. Xu, H. Liu, J. Huang, X. Yao, MolAICal: a soft tool for 3D drug design of protein targets by artificial intelligence and classical algorithm. *Briefings in Bioinformatics*, 00 (2020) 1-12.

[36] S.E. Adeniji, S. Uba, A. Uzairu, QSAR modeling and molecular docking analysis of some active compounds against mycobacterium tuberculosis receptor (Mtb CYP121). *Journal of Pathogens,* (2018) 24-64.

[37] F.A. Ugbe, G.A. Shallangwa, A. Uzairu, I. Abdulkadir, A 2-D QSAR modeling, molecular docking study and design of 2-Arylbenzimidazole derivatives as novel leishmania inhibitors: A molecular dynamics study. *Adv. J. Chem. A*, 6(1) (2023) 50-64.

[38] M.T. Ibrahim, A. Uzairu, S. Uba, G.A. Shallangwa, Design of more potent quinazoline derivative EGFRWT inhibitors for the treatment of NSCLC: a computational approach. *Future Journal of Pharmaceutical Sciences,* 7 (2021) 140. https://doi.org/10.1186/s43094-021-00279-3.

HOW TO CITE THIS ARTICLE

Fabian Audu Ugbe, Gideon Adamu Shallangwa, Adamu Uzairu, Ibrahim Abdulkadir, Combined QSAR Modeling, Molecular Docking Screening, and Pharmacokinetics Analyses for the Design of Novel 2, 6-Diarylidene Cyclohexanone Analogs as Potent Anti-Leishmanial Agents, Prog. Chem. Biochem. Res, 6(1) (2023) 11-30.

DOI: 10.22034/pcbr.2022.366493.1234

URL: http://www.pcbiochemres.com/article_165482.html